Microstructural quantification of collagen fiber orientations and its integration in constitutive modeling of the porcine carotid artery

P. Sáez[§a,d], A. García[§a,e], E. Peña[a,b], T. C. Gasser[c], M. A. Martínez[a,b,*]

[a] *Applied Mechanics and Bioengineering. Aragón Institute of Engineering Research (I3A). University of Zaragoza. Zaragoza. Spain*
[b] *CIBER de Bioingeniería, Biomateriales y Nanomedicina (CIBER-BBN). Zaragoza. Spain*
[c] *Department of Solid Mechanics. Royal Institute of Technology. Stockholm. Sweden*
[d] *Department of Biomedical Engineering, Carnegie Mellon University, Pittsburgh, PA, 15213, United States of America.*
[e] *Department of Chemistry, Materials and Chemical Engineering "Giulio Natta", Politecnico di Milano, Italy*

Abstract

Background: Mechanical characteristics of vascular tissue may play a role in different arterial pathologies, which, amongst others, requires robust constitutive descriptions to capture the vessel wall's anisotropic and non-linear properties. Specifically, the complex 3D network of collagen and its interaction with other structural elements has a dominating effect of arterial properties at higher stress levels. The aim of this study is to collect quantitative collagen organization as well as mechanical properties to facilitate structural constitutive models for the porcine carotid artery. This helps the understanding of the mechancis of swine carotid arteries, being a standard in clinical hypothesis testing, in endovascular preclinical trials for example.

Method: Porcine common carotid arteries (n=10) were harvested and used to (i) characterize the collagen fiber organization with polarized light microscopy, and (ii) the biaxial mechanical properties by inflation testing. The collagen organization was quantified by the Bingham orientation density function (ODF), which in turn was integrated in a structural constitutive model of the vessel wall. A one-layered and thick-walled model was used to estimate mechanical constitutive parameters by least-square fitting the recorded in-vitro inflation test results. Finally, uniaxial data published elsewhere were used to validate the mean collagen organization described by the Bingham ODF.

Results: Thick collagen fibers, i.e. the most mechanically relevant structure, in the common carotid artery are dispersed around the circumferential direction. In addition, almost all samples showed two distinct families of collagen fibers at different elevation, but not azimuthal, angles. Collagen fiber organization could be accurately represented by the Bingham ODF ($\kappa_{1,2,3}$=[13.5,0.0,25.2] and $\kappa_{1,2,3}$=[14.7,0.0,26.6]; average error of about 5%), and their integration into a structural constitutive model captured the inflation characteristics of individual carotid artery samples. Specifically, only four mechanical parameters were required to reasonably (average

*Corresponding author. Tel.: +34876555252; Fax: +34976762578
Email address: miguelam@unizar.es (M. A. Martínez)

error from 14% to 38%) cover the experimental data over a wide range of axial and circumferential stretches. However, it was critical to account for fibrilar links between thick collagen fibers. Finally, the mean Bingham ODF provide also good approximation to uniaxial experimental data.
Conclusions: The applied structural constitutive model, based on individually measured collagen orientation densities, was able to capture the biaxial properties of the common carotid artery. Since the model required coupling amongst thick collagen fibers, the collagen fiber orientations measured from polarized light microscopy, alone, seem to be insufficient structural information. Alternatively, a larger dispersion of collagen fiber orientations, that is likely to arise from analyzing larger wall sections, could have had a similar effect, i.e. could have avoided coupling amongst thick collagen fibers.
Keywords: Collagen distribution, Carotid artery, polarized light, Micro-sphere

---

§ These two authors contributed equally to this work.

1. Introduction

Although health care systems have made great strides in reducing death rates associated with cardiovascular diseases, vascular events are still ranked amongst the main mortality causes in the western world. It is known that onset and progression of cardiovascular diseases are associated with the alteration of the biomechanical properties of cardiovascular tissues [3]. Consequently, some of the variables describing this mechanical behavior such as stress and strain may play a role in different arterial pathologies or some evolutive processes as tissue growth and remodeling [9, 18].

Mechanical characteristics of vascular tissue may play a role in different arterial pathologies. Besides vascular smooth muscle cells (VSMC), the extracellular matrix proteins collagen and elastin play a central role in the biomechanics of vascular tissue, i.e. their spatial organization and their interaction dominate the macroscopic non-linear vessel properties. While elastin provides elasticity and determines low-strain vessel properties, collagen protects the wall from overtretching and contributes mainly to the walls properties at higher strains [29]. However, the collagen fibers are not individually placed along the arteries, they are connected each other, therefore it is important modeling the contribution of both collagen fibrils and the linkers between them. Most importantly, by a continuous turn over of VSMC and collagen, the tissue microstructure adapts to its mechanical environment/needs (see for example [17]), which naturally has significant implications on the physiological vessel performance. Vessel wall adaptation to mechanical needs also explains the reported intraspecies and interspecies variabilities of structural and mechanical properties [11, 21, 34].

Finite strains constitutive descriptions are needed that reliably capture the vessel wall's anisotropic and non-linear properties. Many constitutive models are based on a strain energy function (SEF), i.e. a mathematical

description of vessel wall properties, which in turn is calibrated to data from experimental vessel wall characterization. While phenomenological SEFs are purely based on mechanical input information, structural SEFs integrate also microstructural histological data. Most importantly, structural SEFs allocate macroscopic stress to different micro-structural components, and are able to link the macroscopic loading to potential cellular responses. Structural SEFs for the vessel wall are based on fiber-reinforced composite concepts, which assume straight and parallel-aligned [16, 33, 40], straight and orientation-dispersed [1, 13], undulated and parallel-aligned [39, 40], or undulated and orientation-dispersed [19, 23] (families of) fibers. Despite the fact that considerable work has been dedicated to develop and numerically implement structural SEFs, only very few studies consistently validated structural SEFs, i.e. by treating histological and mechanical input information strictly separately [12, 15, 26, 37]. In contrast, most studies estimated both histological and mechanical model parameters from mechanical experimental data, i.e. they did not consider appropriate microstructural information.

The ability to get detailed fiber orientation [6, 8, 27] and recruitment [7] data makes structural SEFs all the more relevant, such that structural and mechanical model parameters can be separately identified by histological and mechanical experiments, respectively. Specifically, inflation [35, 38], planar biaxial [20, 24] and uniaxial [11, 32] testing are preferable in-vitro mechanical test protocols for vascular tissue. Here, animal models remain popular in clinical hypothesis testing, where specifically the pig carotid artery has a central role. In the case of stenting techniques, common carotid or coronary swine arteries are broadly employed to test the features of these devices. Additionally, the use of animal tissue allow us to collect a sufficient number of coherent wall specimens, i.e. a sample size large enough for sound statistical data analysis.

The aim of this study is to collect quantitative information of the collagen fiber organization in the wall of the porcine carotid artery. Subsequently, this information is incorporated in a structural SEF, and mechanical model parameters were calibrated by leased-square optimization of model prediction and in-vitro vessel inflation experiments. Due to the applied structural constitutive modeling approach we hypothesize that the estimated material parameters reflect the properties of the microstructural components elastin and collagen. The structural information obtained through this study will not only improve our biomechanical understanding of the carotid artery, but also be helpful input information for continuum biomechanics-based simulations.

2. Material and Methods

2.1. Tissue harvesting

Left and right common carotid arteries (see Figure 1) were dissected from 10 female pigs (mean age: 3.5 months, SD 0.4 months). Animals did not present any pathology and were not used in any other experimental study. The

animals were euthanized under general anesthesia through an intravenous injection of potassium chloride and sodium thiopental, and the carotid arteries were harvested by skilled veterinarians. Mechanical and histological samples preparation started within 24 hours, and until then, the tissue was stored in ion-free PSS (0.9% NaCl) solution at 4 [$^{\circ}C$]. The study was approved by the Ethical Committee for Animal Research of the University of Zaragoza and all procedures were carried out in accordance with the "Principles of Laboratory Animal Care". (86/609/EEC Norm, incorporated into Spanish legislation through the RD 1021/2005).

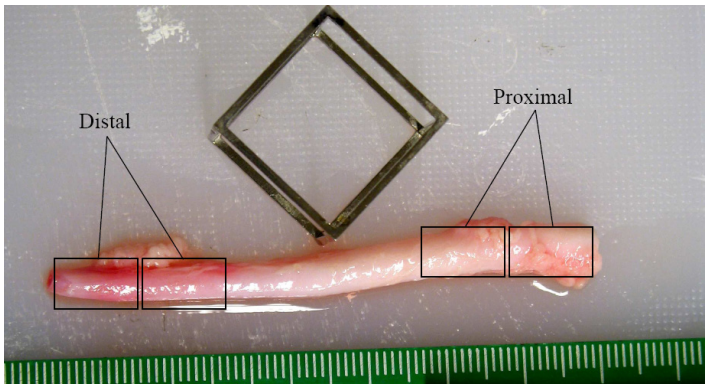

Figure 1: Left common carotid artery specimen. Squares show the proximal and distal regions used for the experiments.

2.2. Mechanical inflation testing

Carotid arteries were tested in an Instron Microtester 5548 system that was adapted for biological tissue testing, such that the tissue remained immersed in ion-free PSS (0.9% NaCl) solution at 37°C at any time. Specially designed vessel diameter-matching tube connectors were used to cannulate the artery segments. Two CCD cameras (Pulnix TM-1405GE) monitored the outer vessel diameter from the front and the lateral side, respectively. Artery segments were stretched axially to 1.2, 1.3 and 1.4 at a time, and then inflated/deflated between 0 and 300 [mmHg] at 2 [mmHg/s]. At each axial stretch level five inflation/deflation cycles were applied to precondition the vessel. Preliminary tests verified that five cycles were sufficient to maintain reproducible experimental recordings. Data from the last cycle was used to identify constitutive model parameters and the vessel relaxed for 300 [s] before the subsequent axial stretch level was set. Axial force and inflation pressure were measured with a 10 [N] load cell at a minimal resolution of 0.002 [N] and an Opsens OPP-B pressure transducer of 0.5 [mmHg] accuracy, respectively. Further details are reported elsewhere [11].

2.3. Collagen histology

Samples (approximately 0.5 × 1.0 cm) from the proximal and distal regions of the left and the right carotid artery were used for collagen histology. Samples were squeezed between two Plexiglas plates (about 5 [min]),

then released and fixed in formaldehyde for 24 [h] before they were moved to 70% alcohol. The applied squeezing induces a homogeneous strain state that (partly) straightens the collagen fibres, especially helpful to perform accurate orientation measurements [12, 31]. Then the segments were further dehydrated, embedded in paraffin, and tangentially sectioned at 7.0 [μm] thickness. In order to enhance the birefringent properties of collagen, which also improves the precision of subsequent collagen orientation measurements, histological sections were stained with Picrosirius red [6]. According to this histological preparation the collagen in the vessel wall appeared bright orange-yellow-red when viewed with polarized light, see Fig. 2. According to these color ranges, it has been assumed that mainly large collagen fibers type I, in addition to dense packs of collagen type III, were analysed by this technique since smaller/thinner fibers mainly appear in the ranges of green-yellow color ranges [12, 41].

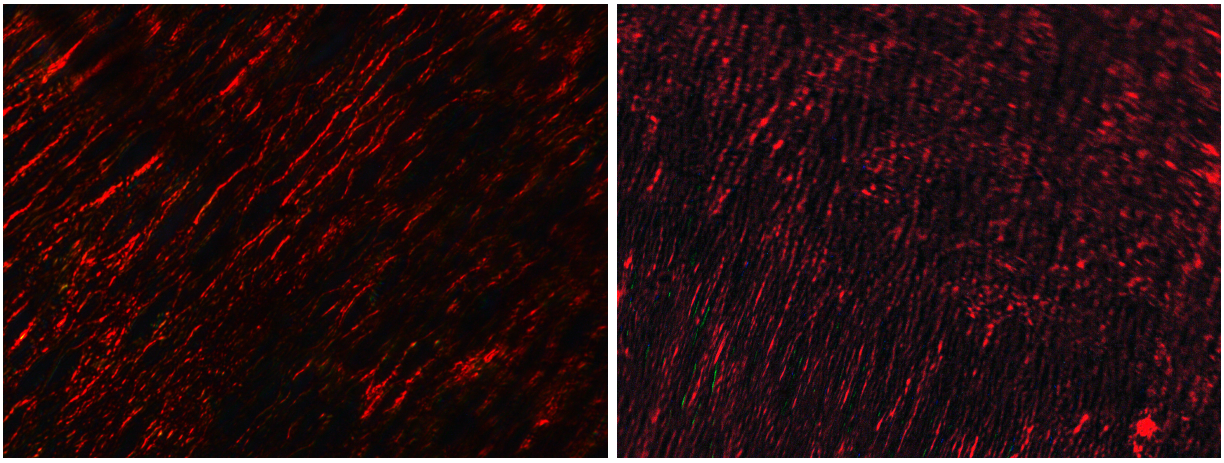

(a) Proximal specimens (b) Distal specimens

Figure 2: Polarized light microscope images taken from the distal (left) and the proximal (right) regions of the left common carotid artery.

A BX50 microscope (Olympus, Melville, USA) equipped with an Achromat UD 16/0.17 objective (16 times magnification; numerical aperture of 0.17) and a CMEX-1300x camera (Euromex microscopen B.V., Arnhem, The Netherlands) was used to analyze the collagen orientation in carotid artery wall. The microscope was equipped with an Universal Rotary Stage (Carl Zeiss GmbH, Jena, Germany) with glass hemispheres of refraction index 1.555, matching the refractive index of collagen, which allowed rotating and tilting the histological section [6]. A thin intervening film of glycerol (refractive index 1.55) was used to eliminate internal reflections in particular at high tilt angles of the stage.

The orientation of a collagen fiber, or a coherent bundle of fibers, in 3D space is uniquely defined by its azimuthal angle Φ and its elevation angle Θ. Azimuthal angles of $\Phi = 90^{\circ}$ and $\Phi = 0^{\circ}$ denote circumferential

and longitudinal directions, respectively. Likewise, an elevation angle of $\Theta = 0^{o}$ denote fibers within the tangential plane and $\Theta = 90^{o}$ specify fibers that are aligned with the radial direction. Both angles were identified by sequentially rotating and tilting the stage until the particular measurement point extinguished in the polarized light microscope. Specifically, for each wall sample collagen orientation measurements were taken at three histological slices across the wall thickness, and at 30 different points at each of these slices. In total of 5040 collagen orientation measurements were taken in this study.

2.4. Validation data

A set of uniaxial tests obtained by the authors in a previous study was used to validate mean collagen organization obtained in this study [11]. The experimental data consists of a simple tension tests of circumferential and longitudinal strips from the proximal and distal parts of porcine carotids. Different loading and unloading cycles were applied: corresponding to 60, 120 and 240 [kPa] at 30%/min of strain rate. Three preliminary cycles at all load levels were applied in order to precondition the sample and the last (fourth) cycle was used for subsequent analysis. For more detail of the experiments, see García et al. [11].

3. Modeling

3.1. Orientation distribution function of the collagen

Besides the Lambert equal area projection [5] also the Bingham orientation distribution function (ODF) [4] was used to analyze the collagen orientation distribution. The Bingham ODF allows to represent a wide range of orientation distributions with the von Mises distribution (for example used in Gasser et al. [13]) being a particular case.

With $\mathbf{r}$ denoting an arbitrary vector in the 3D space, the Bingham ODF reads

$$\rho(\mathbf{r};\mathbf{Z},\mathbf{Q})\frac{dA}{4\pi} = [F_{000}(\mathbf{Z})]^{-1}\exp(\mathrm{tr}(\mathbf{Z}\cdot\mathbf{Q}^{\mathrm{T}}\cdot\mathbf{r}\cdot\mathbf{r}^{\mathrm{T}}\cdot\mathbf{Q}))\frac{dA}{4\pi}, \tag{1}$$

where $\mathbf{Z}$ is a diagonal matrix with eigenvalues $\kappa_{1,2,3}$, $\mathbf{Q}\in\mathbb{Q}^3$ with $A = \mathbf{Q}\cdot\mathbf{Z}\cdot\mathbf{Q}^{t}$. The factor

$$F_{000}(\mathbf{Z}) = \frac{1}{4\pi}\int_{\mathbb{U}^2}\exp(\mathrm{tr}(\mathbf{Z}\cdot\mathbf{r}\cdot\mathbf{r}^{\mathrm{T}}))dA. \tag{2}$$

is introduced so that $1/(4\pi)\int\rho dA = 1$ holds [4, 2].

Consequently, the probability concentration is controlled by the eigenvalues of $\mathbf{Z}$, which in turn can be interpreted as concentration parameters along the three orthogonal directions in space, i.e. along the circumferential, radial and axial vessel wall directions, respectively. Most important, the difference between pairs of eigenvalues, i.e. $\Delta\kappa_{1,2,3} = [\kappa_1-\kappa_2, \kappa_1-\kappa_3, \kappa_2-\kappa_3]$ determines the shape of the distribution. Therefore, one entity of

$\Delta\kappa_{1,2,3}$ may be set to zero without reducing the versatility of the distribution. If two eigenvalues $\Delta\kappa_{1,2,3}$ are set to zero, the Bingham ODF reduces to the classical von Mises ODF [2].

A least-square minimization procedure with the objective function $\chi^2 = \sum_{i=1}^{n}(\rho_i^{exp} - \rho_i^{ODF})^2$ was used in order to estimate Bingham ODF ρ_i^{ODF} parameters from the experimentally identified collagen orientation distribution ρ_i^{exp}. Where $n = 600$ spatial orientations or integration directions discretisation of 39th degree proposed by [14] were used. Accordingly, any continuous integration over the unit sphere can be approximated by a numerical integration

$$\langle(\bullet)\rangle = \frac{1}{4\,\pi}\int_{\mathbb{U}^2}(\bullet)\,\mathrm{d}A \approx \sum_{i=1}^{m} w^i\,(\bullet)_i. \tag{3}$$

where we denote $\{w^i\}_{i=1,\cdots,m}$ the corresponding weighting factors. Each experimentally measured orientation was assigned to the closest spatial orientation of the corresponding numerical integration direction, being p_i the number of experimental orientations assigned to each integration direction i. In order to fulfill the normalization requirements of the numerical integration, $\frac{1}{4\,\pi}\int_{\mathbb{U}^2}\rho_i^{exp}\,\mathrm{d}A \approx \sum_{i=1}^{m} w^i\,\rho_i^{exp}$, the experimental collagen orientation distribution is defined as $\rho_i^{exp} = \frac{p_i}{\hat{p}}$ where $\rho_i^{exp} = \sum_{i=1}^{n}(w^i p_i)$. Finally the quality of the model representation or experimental fitting was assessed by the normalized square error, $NSE = \Sigma_{i=1}^{n}\frac{(\rho_i^{exp}-\rho_i^{ODF})^2}{\rho_i^{exp}}$.

3.2. Inflation test: theoretical framework

In order to mimic the in-vitro inflation experiment the associated equilibrium equations need to be solved. Neglecting body forces this equation reads $div\boldsymbol{\sigma} = 0$, where $div(\bullet)$ is the spatial divergence of $(\bullet)$. In cylindrical coordinates, it yields

$$p_i^{\psi} = \int_{r_i}^{r_o}(\bar{\sigma}_{\theta\theta} - \bar{\sigma}_{rr})\frac{dr}{r}, \qquad F_z^{\psi} = \int_{r_i}^{r_o}(2\bar{\sigma}_{zz} - \bar{\sigma}_{\theta\theta} - \bar{\sigma}_{rr})r dr. \tag{4}$$

Here $\bar{\sigma}_{\theta\theta}, \bar{\sigma}_{rr}$ and $\bar{\sigma}_{zz}$ are the circumferential, radial and longitudinal Cauchy stresses, respectively. r_i and r_o is the internal and external radio of the artery. Given a constitutive model that defines the stresses in eq.4 are expressed, the inflation pressure p_i^{ψ} and axial force F_z^{ψ} can directly be compared to the recordings from the in-vitro inflation experiment [36].

3.3. Uniaxial test: theoretical framework

The tissue was assumed as incompressible, that is $\det(\mathbf{F}) = \lambda_1\lambda_2\lambda_3 = 1$, where $\mathbf{F}$ represents the deformation gradient tensor and λ_i, the stretches in the principal directions. Considering an uniaxial tension test in the longitudinal or circumferential directions, the Cauchy stress tensor becomes $\boldsymbol{\sigma} = [\sigma_{ii},\ 0,\ 0]$ with $i = \theta,\ z$, and one gets,

$$\sigma_{\theta\theta}^{\psi} = \lambda_\theta\frac{\partial\Psi}{\partial\lambda_\theta} \qquad \sigma_{zz}^{\psi} = \lambda_z\frac{\partial\Psi}{\partial\lambda_z}. \tag{5}$$

3.4. Microstructural-based model

We considered the carotid artery wall being a passive, hyperelastic and incompressible material that is reinforced by collagen fibers. Specifically, the additive decomposed SEF per unit reference volume $\Psi = \Psi_{\text{iso}} + \Psi_{\text{ani}}$, described isotropic and anisotropic contributions to the strain energy, respectively. Here, Ψ_{iso} aims at capturing the mechanical properties of the ground matrix material (mainly elastin) and was modeled by the classical neoHookean model $\Psi_{\text{iso}} = C_{10}(I_1 - 3)$. Here, $I_1 = \text{tr}\mathbf{C}$ denotes the first invariant of the right Cauchy Green strain $\mathbf{C} = \mathbf{F}^{\text{T}}\mathbf{F}$ with $\mathbf{F}$ being the deformation gradient.

The anisotropic contribution to the strain energy models the collagen fibers reinforcement and reads

$$\Psi_{\text{ani}} = \frac{1}{4\pi} \int_{\mathbb{U}^2} [\rho + \alpha\hat{\rho}]\psi_{\text{f}} dA, \tag{6}$$

where ρ denotes the Bingham ODF (given by eq.(1)) and ψ_{f} denotes the SEF of the collagen fibers. In addition $\hat{\rho} = [\max(\rho) - \rho]/\max(\rho)$ is an effective orientation density that accounts for cross-links between the main collagen fibers, see Figure 3. $\hat{\rho}$ takes into account the space covered by the collagen cross-links appearing in the physical space where main collagen fibers do not exist, as reported by a previous model [30]. Specifically, $\alpha \in [0, 1]$ represents the relative amount of cross-links with $\alpha = 0$ and $\alpha = 1$ denoting no cross-links and fully cross-linked collagen, respectively. The fully cross-linked state results in an isotropic response of the collagen. Finally, the numerically integration of eq.(6), using $m = 368$ integration points over the unit sphere $\mathbb{U}^2$, gives

$$\Psi_{\text{ani}} = \sum_{i=1}^{m} w_i[\rho_i + \alpha\hat{\rho}_i]\psi_{\text{f}\,i}, \tag{7}$$

with w_i denoting integration point weights.

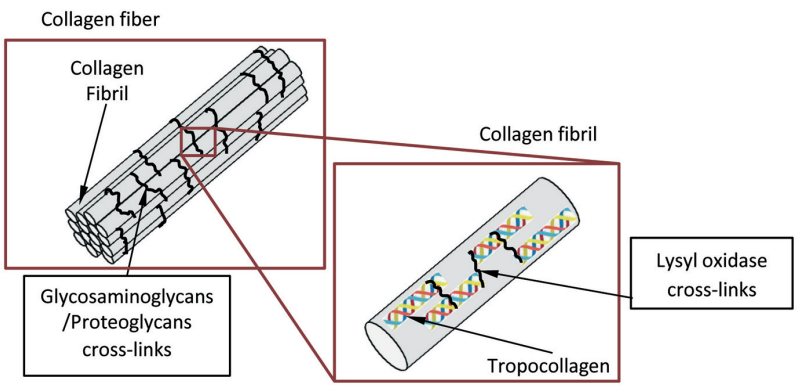

Figure 3: The hierarchical structure of a collagen fibre and cross-links at microfibril level.

We assumed that an individual collagen fiber contributes only in tension to the strain energy and follows the exponential phenomenological model [10, 16]

$$\psi_{\mathrm{f}\,i}(\lambda_i) = \frac{k_1}{2k_2}(e^{k_2((\lambda_i)^2-1)^2} - 1) \quad \text{for} \quad \lambda_i \geq 1 \quad \text{otherwise} \quad \psi_{\mathrm{f}\,i}(\lambda_i) = 0, \tag{8}$$

where affine kinematics defines the collagen fiber stretch $\lambda_i = |\mathbf{t}_i|$, with $\mathbf{t}_i = \mathbf{F}\,\mathbf{r}_i$.

Finally, assuming that the collagen fiber is incompressible, its contribution to the Cauchy stress reads

$$\boldsymbol{\sigma}_i = \rho\lambda^{-1}\psi'_{\mathrm{f}\,i}\,\mathbf{t}\otimes\mathbf{t} \tag{9}$$

with $\psi'_{\mathrm{f}\,i} = \mathrm{d}\psi_{\mathrm{f}\,i}/\mathrm{d}\lambda$.

3.5. Identification of mechanical parameters

Parameter identification was based on a Levenberg-Marquardt type minimization algorithm [22], using the objective functions

$$\chi^2 = \Sigma_{j=1}^{n}\left[\left(w_p(p_i - p_i^{\Psi})\right)_j^2 + \left(w_F(F_z - F_z^{\Psi})\right)_j^2\right], \tag{10}$$

$$\chi^2 = \Sigma_{j=1}^{n}\left[\left(\sigma_{\theta\theta} - \sigma_{\theta\theta}^{\Psi}\right)_j^2 + \left(\sigma_{zz} - \sigma_{zz}^{\Psi}\right)_j^2\right], \tag{11}$$

for inflation and uniaxial tests, respectively. Here, w_p and w_F are weight factors for the internal pressure and the axial force to balance their contributions, and n denotes the number of data points. p_i^{Ψ} and F_z^{Ψ} are the inflation pressure and axial force predicted by eq.4, $\sigma_{\theta\theta}^{\Psi}$ and σ_{zz}^{Ψ} are predicted by eq. 5, whereas p_i, F_z, $\sigma_{\theta\theta}$ and σ_{zz} denote their counterparts measured in the in-vitro experiments.

The goodness of the fitting was quantified by the coefficient of determination of the normalized mean square root errors, i.e.

$$\varepsilon_p = \frac{\sqrt{\frac{\Sigma_{i=1}^{n}\left(p_i - p_i^{\Psi}\right)_i^2}{n-q}}}{\mu_{p_i}} \qquad \text{and} \qquad \varepsilon_{F_z} = \frac{\sqrt{\frac{\Sigma_{i=1}^{n}(F_z - F_z^{\Psi})_i^2}{n-q}}}{\mu_{F_z}}. \tag{12}$$

Here μ_{p_i} and μ_{F_z} denote the mean of the experimentally measured inflation pressures and axial forces, respectively. In addition q is the number of parameters of the SEF, such that $n-q$ denotes the number of degrees of freedom.

4. Results

4.1. Artery dimensions

Wall thickness (range: 0.47 to 0.89 [mm]) and inner diameter (range: 3.46 to 5.12 [mm]) of the unloaded carotid artery samples are shown in Table 1. In all cases, wall thickness ($p = 0.022$) and inner diameter ($p = 0.016$) are higher in the proximal region than in the distal one (0.70 ± 0.13 [mm] and 4.52 ± 0.57 [mm] & 0.52 ± 0.04 [mm] and 3.77 ± 1.26 [mm]).

Specimen	Thickness [mm]	Inner diameter [mm]
PROXIMAL I	0.56	5.12
DISTAL I	0.54	4.10
PROXIMAL II	0.66	5.09
DISTAL II	0.52	3.75
PROXIMAL III	0.63	4.36
DISTAL III	0.47	3.95
PROXIMAL IV	0.70	3.81
DISTAL IV	0.50	3.46
PROXIMAL V	0.89	4.21
DISTAL V	0.58	3.58
ALL PROXIMAL	0.70 (SD 0.13)	4.52 (SD 0.57)
ALL DISTAL	0.52 (SD 0.04)	3.77 (SD 0.26)
ALL SPECIMENS	0.61 (SD 0.13)	4.14 (SD 0.58)

Table 1: Average wall thickness and inner diameter of the unloaded carotid artery samples. There were no significant differences between right and left carotids ($p > 0.05$)

.

4.2. Collagen fibres orientation

Lambert equal area projections of the measured collagen fiber orientations are shown in Figure 4. Lambert equal area projection is stereographic mapping that projects a three-dimensional direction (represented by azimuthal angle Φ and elevation angle Θ) into a point in a two-dimensional plot. Such projections are frequently used in biomechanics [45, 6, 43, 44]. In Figure 4 the azimuthal angle Φ and the elevation angle Θ are represented by the horizontal and vertical axes, respectively. Consequently, a fiber aligned with the circumferential direction ($\Phi = 0$ and $\Theta = 0$) appears as a point in the center of Lambert equal area projection. Specifically, Figure 4 illustrates that collagen in the carotid artery predominantly aligns along the circumferential direction, i.e. measurement points are grouped in the center of the Lambert projections. In addition, almost all samples exhibit two distinct families of collagen fibers with respect to their elevation angle, i.e. vertical axis of the Lambert projection. No such separation is seen with respect to collagen fibers' azimuthal angle, i.e. horizontal axis of the Lambert projection. Quantitative collagen fiber orientation results are given in Table 2, which considered the above described separation into two families of fibers of different mean elevations.

4.3. Bingham representation of the collagen orientation distribution

Figure 5 represents a color-coded plots of the Bingham ODFs that have been fitted to the measured collagen orientations, i.e. that corresponds to the Lambert equal area projections shown in 4. Bingham ODF parameters $\kappa_{1,2,3}$ and NSE are given in Table 2. Due to the observed separation of collagen fibers into families with positive and negative elevations, parameters for both families are presented. The low NSE of about 5% indicates that the introduced Bingham ODFs accurately represents the measured collagen fiber orientations.

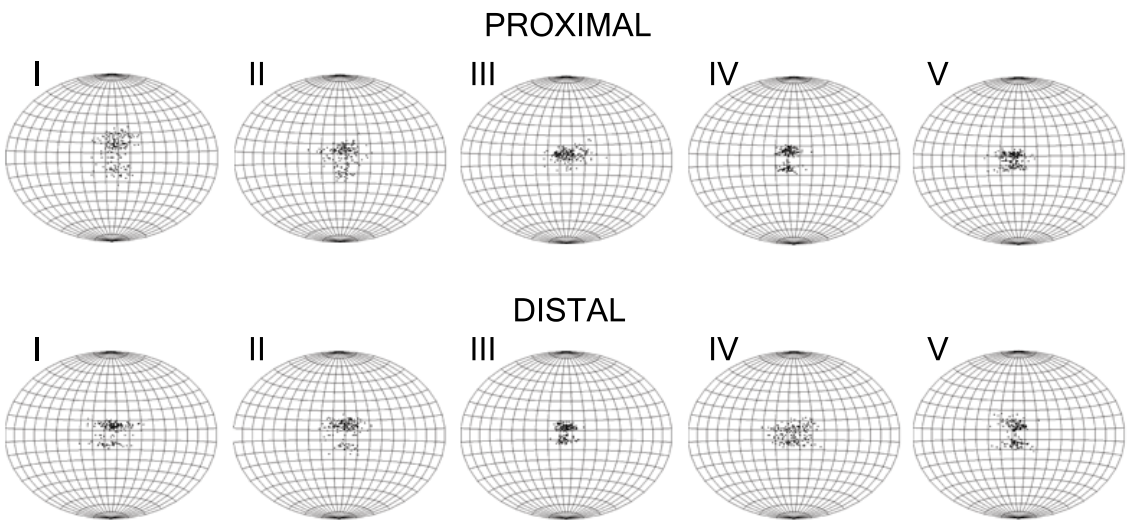

Figure 4: Lambert equal area projections of the collagen fibers orientations in the proximal (top) and distal (bottom) wall of the common carotid artery. Azimuthal angle Φ and elevation angle Θ are represented by the horizontal and vertical axes, such that the circumferential direction (Φ=0 and Θ=0) appears in the center of the stereographic plots. Collagen fibers are predominantly aligned along the circumferential direction (center of the Lambert projection) and almost all samples show two distinct families of fibers with respect to their elevation (vertical axis of the Lambert projection).

4.4. Mechanical constitutive model parameter estimation by inflation test

Mechanical constitutive model parameters were estimated separately for the distal and proximal carotid segments. The estimated parameters including quality of model representation measures are summarized in Table 3. The parameter identification was based on the readings from the in-vitro inflation experiments (see Section 4.4), the dimensions of proximal and distal artery segments (Table 1), and the individual Bingham parameters reported in Table 2. None of the identified mechanical constitutive model parameters differed between distal and proximal segments ($p > 0.05$). In addition Fig. 6 shows overlays of experimental and model-predicted inflation pressure versus circumferential stretch ($p_i - \lambda_\theta$) and axial force versus circumferential stretch ($\mathrm{F}_z - \lambda_\theta$) plots of the inflation test. Model representation of the arteries inflation pressure versus circumferential stretch properties was significantly better than their axial force versus circumferential stretch properties ($\varepsilon_p = 0.19; 0.14$ and $\varepsilon_{F_z} = 0.37; 0.38$, respectively).

4.5. Mechanical constitutive model parameter estimation by uniaxial tensile test

For the validation uniaxial tests, mechanical constitutive model parameters were estimated separately for the distal and proximal carotid segments using the mean Bingham ODF parameters from Table 2. The estimated

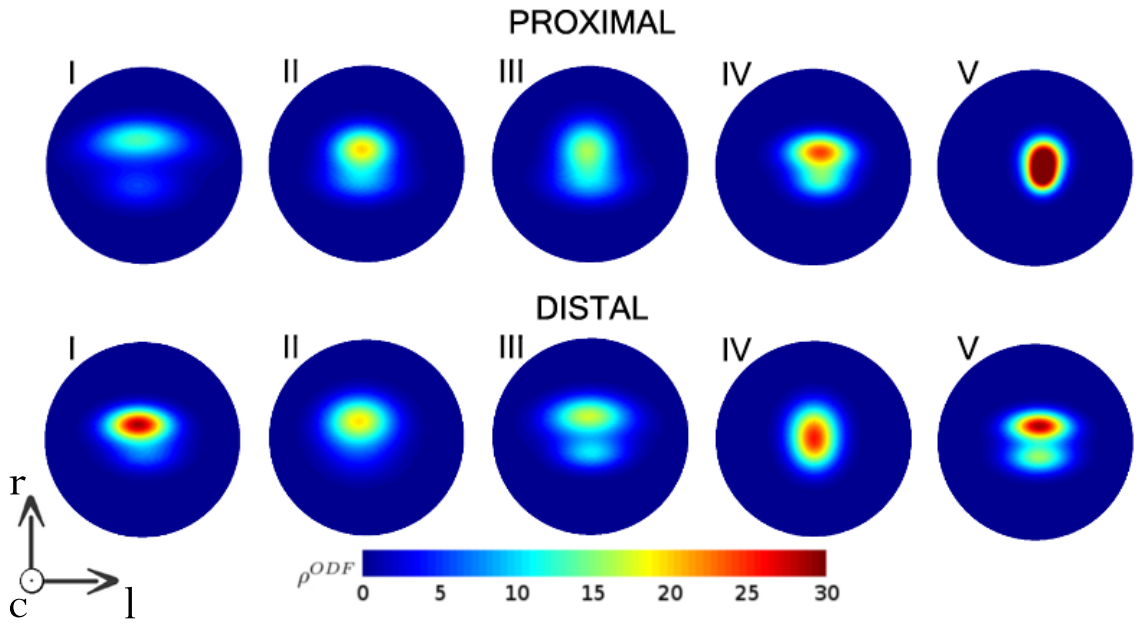

Figure 5: Color-coded and stereographic mapping of the Bingham orientation distribution function (ODF). Azimuthal angle Φ and elevation angle Θ are represented by the horizontal and vertical axes, such that the circumferential direction (Φ=0 and Θ=0) appears in the center of the stereographic plots. Data represent the collagen fibers orientations in the proximal (top) and distal (bottom) wall of the common carotid artery.

parameters including quality of model representation measures are summarized in Tables 4 and 5. The parameter identification was based on the readings from the uniaxial experiments (see Section 2.4). In addition Figs. 7 and 8 show overlays of experimental and model-predicted Cauchy stress versus stretch of the uniaxial test. The values obtained of ε are very low for all the fitted data clearly demonstrating the goodness of the fitting and the validation of the proposed model ($\varepsilon = 0.088$ and $\varepsilon = 0.080$, for proximal and distal specimens respectively).

5. Discussion

In this study, polarized light microscopy and in-vitro inflation experiments were used for histological and mechanical characterizations of the common carotid artery. To this end the measured collagen fiber orientation distribution was integrated in a structural constitutive model of the artery wall, and mechanical model parameters were estimated through least square fitting the recordings from the inflation experiment. Note that type I and densely packed type III collagen fibers show similar wavelengths of color ranges in polarized light microscopy, see [42] and references herein for example. Consequently, the collagen fiber orientations measured in the present study correspond to mainly collagen type I and densely packed type III collagen fibers. These structures are thought being mainly responsible for stiffness and compliance [12] in arteries.

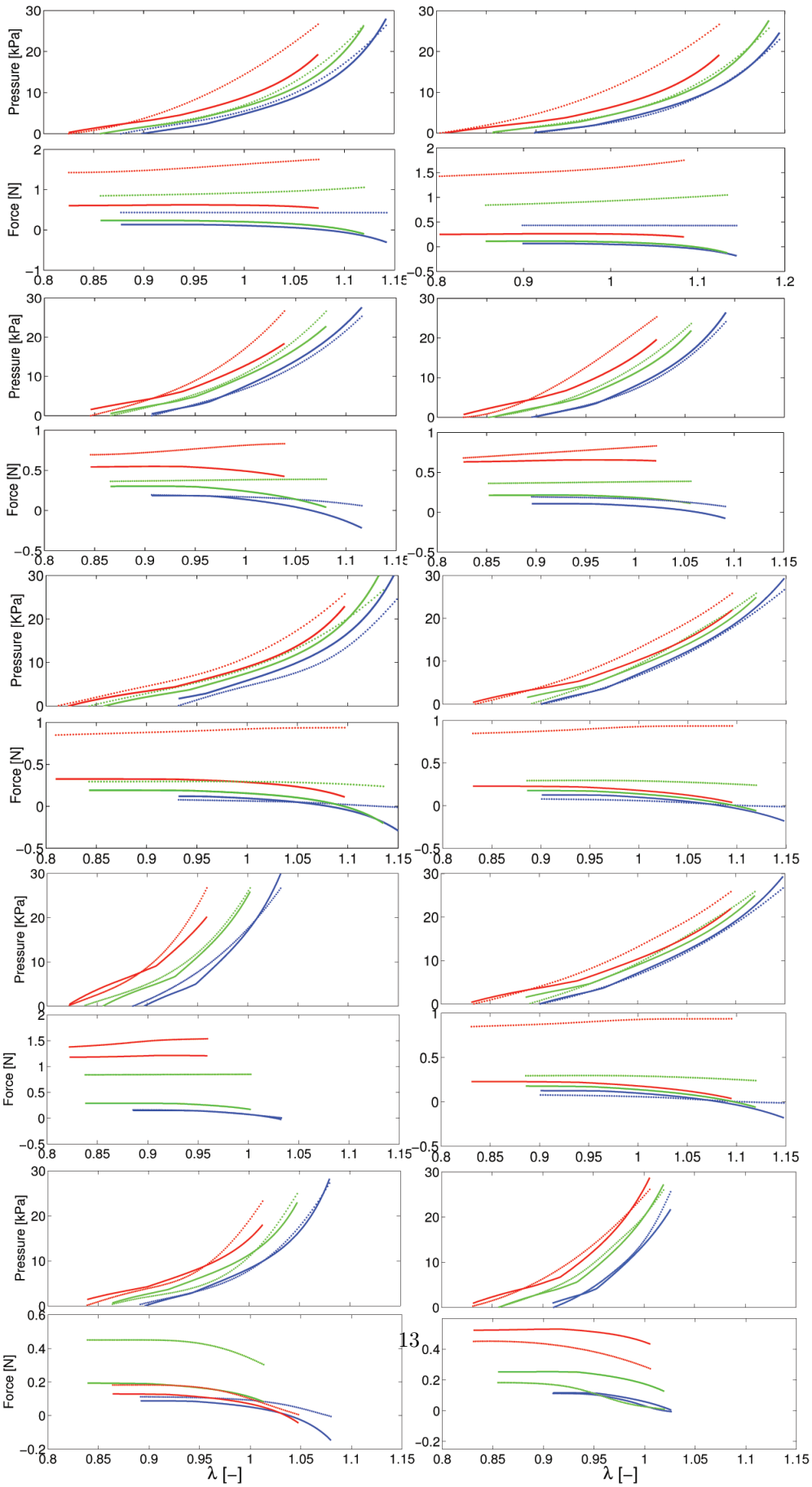

Figure 6: Experimental inflation data at different axial stretches compared to model predictions based on strain-energy function (6). For specimen I-V we show the pressure-λ_θ on top and the force-λ_θ. in the bottom, proximal samples on the left and distal on the right. $\lambda_z = 1.2$ in blue, $\lambda_z = 1.3$ in green and $\lambda_z = 1.4$ in red.

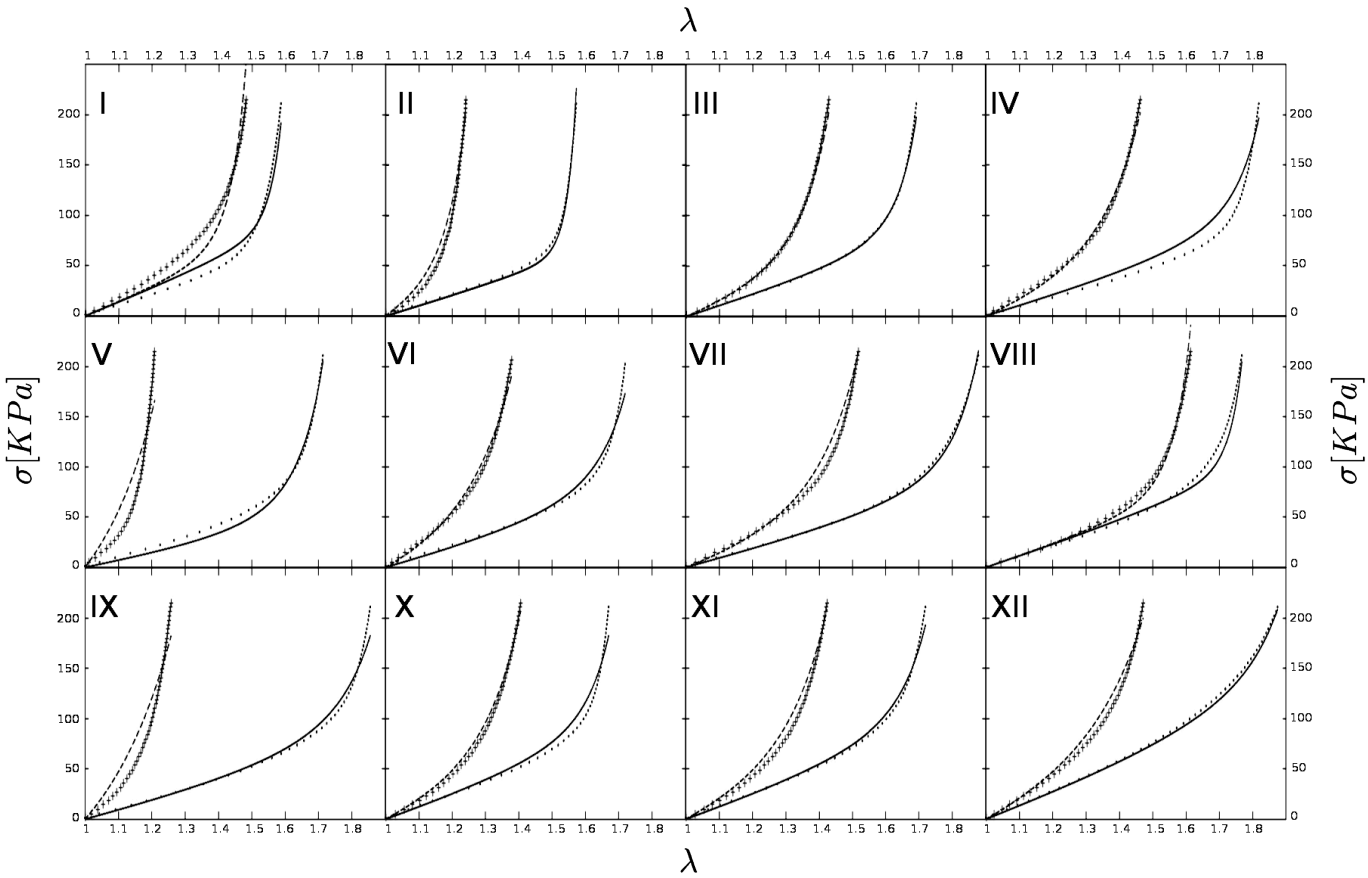

Figure 7: Experimental uniaxial tensile tests of proximal specimens (dashed line for circumferential direction and continuous line for longitudinal direction) compared to model predictions based on strain-energy function (6). Crosses line corresponds to the numerical fitting of the uniaxial tensile test in circumferential direction and the dotted line corresponds to the longitudinal direction.

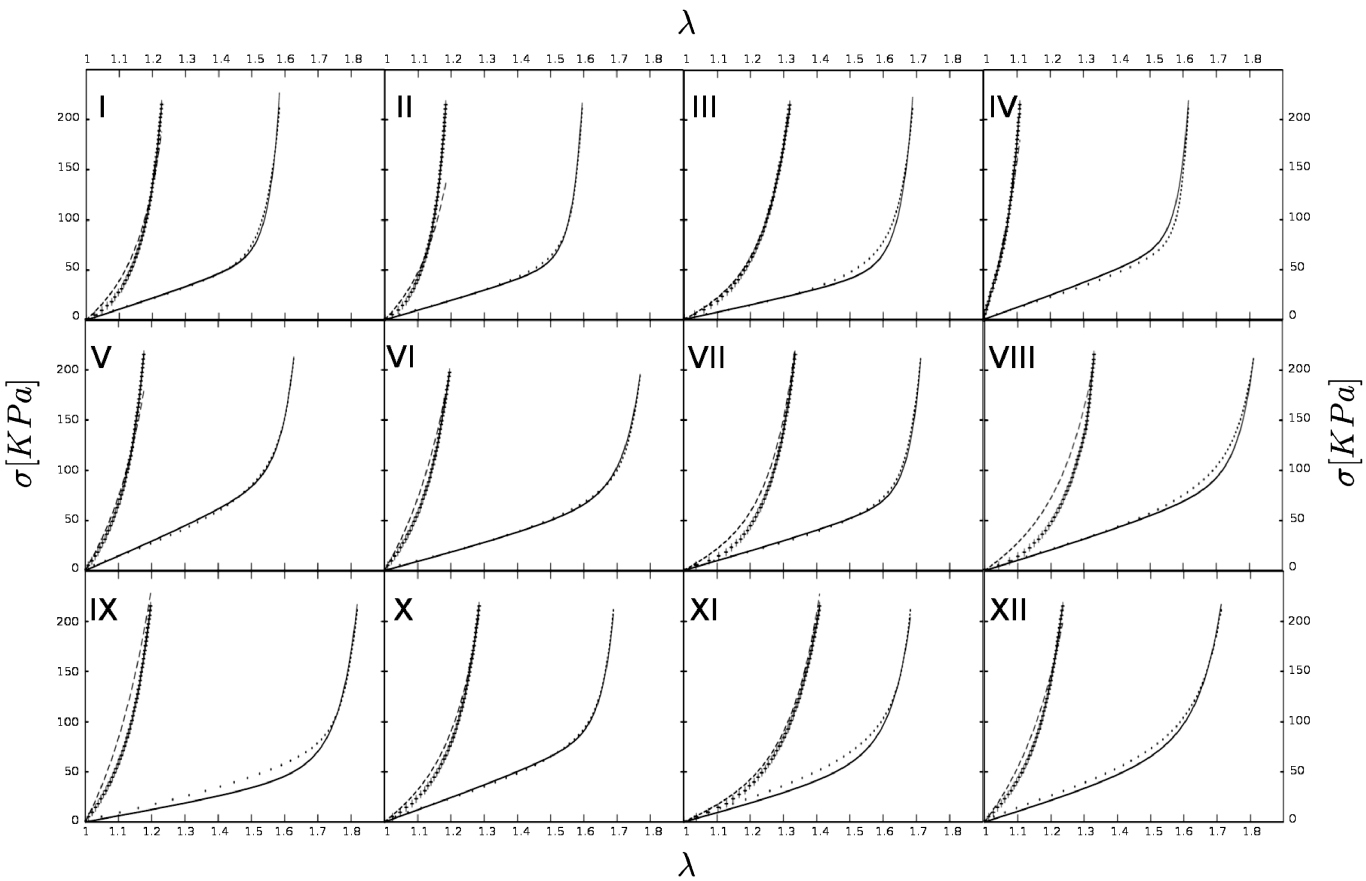

Figure 8: Experimental uniaxial tensile tests of distal specimens (dashed line for circumferential direction and continuous line for longitudinal direction) compared to model predictions based on strain-energy function (6). Crosses line corresponds to the numerical fitting of the uniaxial tensile test in circumferential direction and the dotted line corresponds to the longitudinal direction.

	Family of collagen fibers with positive elevation				Family of collagen fibers with negative elevation			
	$\overline{\phi}$ (SD)	$\overline{\theta}$ (SD)	$\kappa_{1,2,3}$	NSE $\times 10^{-2}$	$\overline{\phi}$ (SD)	$\overline{\theta}$ (SD)	$\kappa_{1,2,3}$	NSE $\times 10^{-2}$
PROXIMAL I	93.6 (7.0)	15.2 (6.0)	[20.4,0.0,24.7]	4.1	93.4 (7.3)	12.3 (4.7)	[15.3,0.0,21.3]	5.0
DISTAL I	92.5 (7.3)	9.0 (2.4)	[27.1,0.0,37.2]	5.1	88.4 (7.9)	8.3 (2.7)	[24.0,0.0,33.1]	4.3
PROXIMAL II	92.8 (8.1)	8.9 (4.1)	[10.3,0.0,21.6]	4.5	93.0 (5.8)	11.0 (5.8)	[23.0,0.0,30.0]	4.7
DISTAL II	94.6 (7.3)	10.1 (3.5)	[8.6,0.0,17.6]	5.1	94.6 (6.9)	10.9 (3.8)	[9.2,0.0,16.6]	5.1
PROXIMAL III	91.9 (8.0)	6.3 (3.4)	[3.5,0.0,30.0]	5.1	91.2 (7.8)	4.8 (3.4)	[3.5,0.0,30.0]	4.4
DISTAL III	89.6 (4.1)	7.8 (2.5)	[48.1,0.0,64.0]	7.3	89.5 (4.9)	4.7 (2.2)	[0.0,0.0,52.1]	6.4
PROXIMAL IV	85.9 (4.5)	9.1 (2.6)	[24.1,0.0,34.0]	7.1	85.3 (4.5)	7.9 (2.3)	[21.2,0.0,34.2]	6.1
DISTAL IV	89.8 (9.4)	7.4 (3.7)	[0.0,0.0,17.1]	4.3	89.5 (8.4)	6.4 (3.0)	[0.0,0.0,20.4]	4.1
PROXIMAL V	84.8 (6.5)	5.8 (2.2)	[0.0,0.0,29.3]	5.9	85.6 (6.2)	5.6 (2.7)	[0.0,0.0,46.2]	6.0
DISTAL V	87.6 (5.7)	9.5 (3.9)	[38.5,0.0,50.0]	5.5	87.9 (5.9)	8.9 (2.9)	[14.7,0.0,26.6]	5.3
ALL PROXIMAL	90.0 (8.5)	8.7 (5.0)	[9.6,0.0,22.4]	5.3	89.0 (7.5)	8.8 (5.0)	[18.6,0.0,30.3]	5.2
ALL DISTAL	91.8 (7.8)	8.8 (3.8)	[18.6,0.0,30.6]	5.5	90.8 (8.3)	7.7 (3.5)	[15.0,0.0,28.4]	5.0
ALL SPECIMENS	91.0 (8.2)	8.8 (4.4)	[13.5,0.0,25.2]	5.4	89.9 (8.0)	8.3 (4.3)	[14.7,0.0,26.6]	5.1

Table 2: Collagen fiber orientation in the common carotid artery wall. Mean and standard deviation (SD) of collagen fiber elevation $\overline{\phi}$ and azimuthal $\overline{\theta}$ for individual wall samples. Bingham ODF parameters are denoted by $\kappa_{1,2,3}$ and NSE denotes the normalized square error of the model representation.

	C_{10} [kPa]	k_1 [kPa]	k_2	α	ε_p	ε_{F_z}
PROXIMAL I	13	11	4	0.4	0.22	0.8
DISTAL I	8	9	3	0.3	0.19	0.93
PROXIMAL II	16	7	3	0.4	0.22	0.4
DISTAL II	15	18	4	0.5	0.19	0.42
PROXIMAL III	25	15	2	0.2	0.23	0.69
DISTAL III	16	7	3	0.5	0.22	0.61
PROXIMAL IV	18	15	5	0.45	0.17	0.31
DISTAL IV	20	17	5	0.5	0.31	0.48
PROXIMAL V	9	4	3	0.25	0.18	0.54
DISTAL V	16	19	5	0.2	0.17	0.51
ALL PROXIMAL	16.20 (SD 5.97)	10.40 (SD 4.87)	3.40 (SD 1.14)	0.34 (SD 0.11)	0.20 (SD 0.03)	0.55 (SD 0.20)
ALL DISTAL	15 (SD 4.35)	14 (SD 5.56)	4 (SD 1)	0.40 (SD 0.14)	0.05 (SD 0.22)	0.59 (SD 0.20)
ALL SPECIMENS	15.6 (SD 4.97)	12.2 (SD 5.29)	3.7 (SD 1.06)	0.37 (SD 0.12)	0.22 (SD 0.06)	0.57 (SD 0.19)

Table 3: Estimated mechanical constitutive model parameters. Parameter C_{10} reflects the ground material (elastin mainly) properties, k_1 and k_2 define collagen fiber properties, and α determines the collagen fiber cross-linking level. The quality of the model representation is characterized by ε_p and ε_{F_z}.

Our histological results showed that the collagen fiber orientation in predominantly aligned along the vessel's circumferential direction with significant dispersion around this direction. Our data was based on analyzing a rather small area of the histological slices, and the dispersion is expected to increase when increasing the analyzing area, which, however, would require automatic methods, see for example [26]. We could not observe different families of collagen fibers with respect to the azimuthal angles, as it has been postulated previously in the literature for other vessels [13]. In addition, our study did not reveal significant differences in the collagen organization between proximal and distal locations. However, the collagen orientations were grouped at two different elevations in almost all investigated wall samples. Despite the fact this finding remains one to some

	C_{10} [kPa]	k_1 [kPa]	k_2	α	ε
I	23.0	0.5	3.0	0.995	0.140
II	17.0	23.0	4.2	0.005	0.076
III	18.0	6.0	1.4	0.350	0.045
IV	17.0	7.8	0.8	0.270	0.085
V	11.0	57.5	1.0	0.110	0.141
VI	15.7	15.0	0.850	0.390	0.082
VII	15.2	6.0	0.7	0.3	0.065
VIII	19.0	0.230	1.760	0.5	0.092
IX	15.0	45.0	0.530	0.090	0.137
X	20.0	9.5	1.150	0.5	0.0787
XI	20.0	10.0	0.9	0.5	0.075
XII	22.0	9.0	0.5	0.350	0.056
Mean	17.5	9.25	0.95	0.35	0.080
SD	3.33	17.82	1.11	0.25	0.032

Table 4: Estimated mechanical constitutive model parameters for proximal uniaxial tests. Parameter C_{10} reflects the ground material (elastin mainly) properties, k_1 and k_2 define collagen fiber properties, and α determines the collagen fiber cross-linking level. The quality of the model representation is characterized by ε.

	C_{10} [kPa]	k_1 [kPa]	k_2	α	ε
I	18.0	30.0	3.500	0.010	0.084
II	16.0	40.0	3.500	0.005	0.185
III	12.0	16.0	2.200	0.020	0.047
IV	20.0	155.0	3.250	0.001	0.120
V	24.0	65.0	2.400	0.010	0.076
VI	15.0	72.0	1.300	0.010	0.079
VII	16.0	13.0	2.200	0.010	0.081
VIII	8.0	45.0	0.250	0.500	0.380
IX	10.0	89.0	1.100	0.010	0.149
X	20.0	22.0	2.200	0.010	0.049
XI	15.0	9.0	1.400	0.330	0.067
XII	17.0	50.500	1.100	0.085	0.077
Mean	15.5	37.5	1.975	0.01	0.088
SD	4.14	39.5	0.97	0.15	0.087

Table 5: Estimated mechanical constitutive model parameters for distal uniaxial tests. Parameter C_{10} reflects the ground material (elastin mainly) properties, k_1 and k_2 define collagen fiber properties, and α determines the collagen fiber cross-linking level. The quality of the model representation is characterized by ε.

extent on the recently observed tilting of smooth muscle cells in the media [25], the reason and implication behind it remain unclear. Specifically, it cannot be excluded that this reflects an artefact from pooling the measurements that were taken from the individual histological sections. Consequently, alternative approaches that avoid pooling section-specific measurements and analyze the wall structure of an intact 3D section, like methods based on confocal laser scanning microscopy [28] or nonlinear multiphoton microscopy [37], could have advantages.

Finally, it is worth mentioning that in order to simplify the experimental analysis and mechanical characterization, the tissue was considered as mono-layer, assuming the media layer being responsible for the mechanical response of swine carotid arteries within the tested range of deformations, being the one with much higher density of collagen fibers compared to adventitia or intima layers [31]. Therefore the analysed histologies corresponded mainly to media layer locations, nevertheless the position in depth of the histologies was not measured, so it is not possible to evaluate the depth dependence of collagen orientation directions. However, no visual significative differences were found in any of the analysed histologies. Further analyses could be carried out by differentiating layers and recording depth of histologies in order to obtain more accurate results. On the other hand, the presented numerical fitting of the mechanical response of in-vitro inflation experiments showed a rather good accuracy with this monolayer assumption. Interestingly in this respect was also the observation that the proposed one-layer inflation model predicted considerably better the vessel's pressure-circumferential stretch properties than its axial force-circumferential stretch properties. Clear reasons for this observation remain unknown. However, recent work [34] indicated that the predictability of inflation tests can be improved by considering anisotropy of the elastin-related stress in the vessel wall, such as refining our constitutive model in that respect is recommended.

The identified collagen orientation densities were integrated in a micro-sphere-based constitutive model, which after calibration was able to reasonably reproduce the experimental inflation test results. Noticeably, distal vessel properties were similar to proximal properties, and model predictions reproduced considerably better the vessel's inflation pressure-circumferential stretch than its axial force-circumferential stretch properties. Similar observations have already been reported in the literature, see for example [34, 35]. Finally, we mentioned that considering cross-linking among the collagen fibers ($\alpha > 0$) was essential for the constitutive model to capture the experimental data. As described previously by [30], the cross-links between the main collagen fibers contribute to the compliance of the tissue. Based on previous models, the mechanical contribution in the longitudinal direction could not be observed in cases where the main fibers are preferentially aligned in circumferential behavior, as in the present study.

A set of uniaxial tests provided by another previous study was used to validate the mean collagen organization described by the Bingham ODF and the model captures the mechanical behavior of carotids $\varepsilon = 0.08$. The capability of the model to reproduce the mechanical behavior of another different set of experiments to the one used to fit the Bingham distribution are demonstrated.

Despite the applied approach tried to use state-of-the-art methods, several limitations should be mentioned. Most importantly, the arterial wall's multilayered structure was approximated by a one-layered homogeneous model without residual strains in the unloaded configuration. However, it is expected that the wall properties change across the thickness, such that the estimated mechanical model parameters in this study only reflect

surrogate biomechanical information. Similarly, we used only three histological sections across the wall to identify the collagen organization, which would have overlooked potential gradual changes, i.e. as recently reported for the porcine aorta [26], for example. Consequently, a refined analysis should explore the radial inhomogeneity of both, collagen histology and mechanical wall properties, respectively.

Our polarized light microscopy identified only thicker collagen fibers, but the vascular wall included also finer collagen fiber structures [25], which also could be mechanically relevant. Interestingly, these finer structures seem to cross-bridge thicker fibers in a mesh-like network without a clear preferred fiber orientation. In the present study such a coupling amongst thicker collagen fibers it is thought to be captured by the previously suggested coupling parameter α [30]. However, since the level of mechanical coupling can not be histologically identified, α was considered as an unknown in the parameter estimation procedure, i.e. identified through least-square fitting experimental inflation data. In this direction, further structural investigations are needed toward the identification of the cross-links parameter.

Inflation mechanical testing has been used to characterize the common carotid artery properties. This protocol allows independent control over a wide range of axial and circumferential wall stretches, and, amongst the suggested in-vitro experimental techniques, it is probably the protocol that is closest to in-vivo artery conditions. In order to minimize edge effects from specimen mounting the inflation tests were performed with the whole common carotid artery, and for the analytical analysis the axial stretch was regarded constant along the rather long vessel. However, since vessel histology is markedly different between the muscular distal and the elastic proximal segments (see for example [9, 11, 18, 21]), also the axial stretch could be inhomogeneous distributed amongst them. Separate read-outs for distal and proximal segments with optical markers, for example, could avoid this draw-back in our study and perhaps improve the reported results. Despite the fact that a multilayer mechanical analysis of the vessel wall is desired it is barely impossible to separate the vessel into different concentric layers and perform inflation test on these layers separately.

Data provided in this study relate to the porcine carotid artery, which clearly cannot directly be translated to human carotids. However, the very same method applied in the present work should also be applicable to explore human carotid arteries. Specifically, due to qualitative similarities between human and porcine vessels, it is expected that the very same mathematical framework is applicable, i.e. the proposed models to capture the vessel's collagen organization and its mechanics could also be calibrated to human data.

6. Conclusions

The present study found that thick collagen fibers in the porcine common carotid artery are dispersed around the circumferential direction. Integrating this information in a structural constitutive model allowed it to reflect the inflation characteristics of individual carotid artery samples. Specifically, only four mechanical parameters were

required to cover the experimental data reasonable over a wide range of axial and circumferential stretches. Noticeably, the coupling parameter α (one out of these four parameters) was critical for reasonable model predictions, such that the collagen fiber orientation measurements from polarized light microscopy, alone, seem to be insufficient structural information. To the authors knowledge this is the first study of the carotid artery that integrates separately identified collagen fiber orientations in a structural constitutive model to predict the artery inflation characteristics.

7. Acknowledgements

Financial support for this research was provided by the Spanish Ministry of Economy and Competitiveness through research project DPI2013-44391-P and the Instituto de Salud Carlos III (ISCIII) through the CIBER initiative. Finally, we also thank the Spanish Ministry of Science and Technology for the financial support to A. García (BES-2008-002951) and to P. Sáez (BES-2009-028593).

[1] Alastrué, V., Martínez, M. A., Doblaré, M., Menzel, A., 2009. Anisotropic micro-sphere-based finite elasticity applied to blood vessel modelling. J Mech Phys Solids 57, 178–203.

[2] Alastrué, V., Saez, P., Martínez, M. A., Doblaré, M., 2010. On the use of bingham statistical distribution in microsphere-based constitutive models of arterial tissue. Mech Res Commun 37, 700–706.

[3] Bäck, M., Gasser, T., Michel, J.-B., Caligiuri, G., 2013. Review. biomechanical factors in the biology of aortic wall and aortic valve diseases. Cardiovasc. Res. 99, 232–241.

[4] Bingham, C., 1974. An antipodally summetric distribution on the sphere. Ann Stat 2, 1201–1225.

[5] Borradaile, G. J., Borradaile. Statistics of Earth science data. Berlin: Springer-Verlag.

[6] Canham, P. B., Finlay, H. M., Dixon, J. G., Boughner, D. R., Chen, A., 1989. Measurements from light and polarised light microscopy of human coronary arteries fixed at distending pressure. Cardiovasc Res 23, 973–982.

[7] Fata, B., Carruthers, C. A., Gibson, G., Watkins, S. C., Gottlieb, D., Mayer, J. E., Sacks, M. S., 2013. Regional structural and biomechanical alternations of the ovine main pulmonary artery during postnatal growth. J. Biomech. Eng. 135, 021022–1–021022–11.

[8] Finlay, H. M., McCullough, L., Canham, P. B., 1995. Three-dimensional collagen organization of human brain arteries at different transmural pressures. J Vasc Res 32, 301–312.

[9] Fung, Y. C., 1993. Biomechanics. Mechanical properties of living tissues. Springer-Verlag.

[10] Fung, Y. C., 1967. Elasticity of soft tissues in simple elongation. Am. J. Physiol. 213, 1532–1544.

[11] García, A., Peña, E., Laborda, A., Lostalé, F., Gregorio, M. A. D., Doblaré, M., Martínez, M. A., 2011. Experimental study and constitutive modelling of the passive mechanical properties of the porcine carotid artery and its relation to histological analysis. Implications in animal cardiovascular device trials. Med Eng Phys 33, 665–676.

[12] Gasser, T. C., Gallinetti, S., Xing, X., Forsell, C., Swedenborg, J., Roy, J., 2012. Spatial orientation of collagen fibers in the abdominal aortic aneurysm's wall and its relation to wall mechanics. Acta Biom 8, 3091–3103.

[13] Gasser, T. C., Ogden, R. W., Holzapfel, G. A., 2006. Hyperelastic modelling of arterial layers with distributed collagen fibre orientations. J R Soc Interface 3, 15–35.

[14] Heo, S., Xu, Y., 2001. Constructing fully symmetric cubature formulae for the sphere. Math Comput 70, 269–279.

[15] Hollander, Y., Durban, D., Lanir, Y., 2011. Experimentally validated microstructural 3D constitutive model of coronary arterial media. J Biomech Eng 61, 1–48.

[16] Holzapfel, G. A., Gasser, T. C., Ogden, R. W., 2000. A new constitutive framework for arterial wall mechanics and a comparative study of material models. J Elasticity 61, 1–48.

[17] Humphrey, J. D., 1995. Mechanics of the arterial wall: Review and directions. Crit Rev Biomed Eng 23, 1–162.

[18] Humphrey, J. D., 2002. Cardiovascular Solid Mechanics: Cells, Tissues, and Organs. Springer-Verlag, New York.

[19] Lanir, Y., 1979. A structural theory for the homogeneous biaxial stress-strain relationship in flat collageneous tissues. J Biomech 12, 423–436.

[20] Lanir, Y., Fung, Y. C., 1974. Two-dimensional mechanical properties of rabbit skin-I. Experimental system. J. Biomech. 7, 29–34.

[21] Mangell, P., Länne, T., Sonesson, B., Hansen, F., Bergqvist, D., 1996. Regional differences in mechanical properties between major arteries: An experimental study in sheep. Eur J Vasc Endovasc Surg 12, 189–195.

[22] Marquardt, D. W., 1963. An algorithm for least-squares estimation of nonlinear parameters. Siam J Appl Math 11, 431–441.

[23] Martufi, G., Gasser, T. C., 2011. A constitutive model for vascular tissue that integrates fibril, fiber and continuum levels. J. Biomech. 44, 2544–2550.

[24] Nielsen, P. M. F., Hunter, P. J., Smaill, B. H., 1991. Biaxial testing of membrane biomaterials: testing equipment and procedures. J. Biomech. Eng. 113, 295–300.

[25] O'Connell, M. K., Murthy, S., Phan, S., Xu, C., Buchanan, J., Spilker, R., Dalman, R. L., Zarins, C. K., Denk, W., and Taylor, C. A. (2008). The three-dimensional micro- and nanostructure of the aortic medial lamellar unit measured using 3D confocal and electron microscopy imaging. *Matrix Biol*, 27(3):171–181.

[26] Polzer, S., Gasser, T., Novak, K., Man, V., Tichy, M., Skacel, P., Bursa, J., 2014. Structure-based constitutive model can accurately predict planar biaxial properties of aortic wall tissue. Acta Biomaterialia (in press).

[27] Polzer, S., Gasser, T., Forsell, C., Druckmullerova, H., Tichy, M., Vlachovsky, R., Bursa, J., 2013. Automatic identification and validation of planar collagen organization in the aorta wall with application to abdominal aortic aneurysm. Micros. Microanal. 19, 1395–1404.

[28] Rezakhaniha, R., Agianniotis, A., Schrauwen, J. T. C., Griffa, A., Sage, D., Bouten, C. V. C., van de Vosse, F. N., Unser, U., Stergiopulos, N., 2012. Experimental investigation of collagen waviness and orientation in the arterial adventitia using confocal laser scanning microscopy. Biomech Model Mechanobiol 11, 461–473.

[29] Roach, M. R., Burton, A. C., 1957. The reason for the shape of the distensibility curve of arteries. Canad. J. Biochem. Physiol. 35, 681–690.

[30] Saez, P., Pena, E., Martinez, M.A. A structural approach including the behavior of collagen cross-links to model patient-specific human carotid arteries. Ann Biomed Eng. 42(6):1158-69.

[31] Schriefl, A., Zeindlinger, G., Pierce, D., Regitnig, P., Holzapfel, G. A., 2012. Determination of the layer-specific distributed collagen fiber orientations in human thoracic and abdominal aortas and common iliac arteries. J R Soc Interface 9, 1275–1286.

[32] Silver, F. H., Snowhill, P. B., Foran, D. J., 2003. Mechanical Behavior of Vessel Wall: A Comparative Study of Aorta, Vena Cava, and Carotid Artery. Ann Biomed Eng 31, 793–803.

[33] Sokolis, D. P., 2010. A passive strain-energy function for elastic and muscular arteries: correlation of material parameters with histological data. Med Biol Eng Comput 48, 507–518.

[34] Sokolis, D. P., Sassani, S., Kritharis, E. P., Tsangaris, S., 2011. Differential histomechanical response of carotid artery in relation to species and region: mathematical description accounting for elastin and collagen anisotropy. Med Biol Eng Comput 49, 867–879.

[35] Sommer, G., Regitnig, P., Koltringer, L., Holzapfel, G. A., 2010. Biaxial mechanical properties of intact and layer-dissected human carotid arteries at physiological and supra-physiological loadings. Am J Physiol Heart Circ Physiol 298, H898–912.

[36] Taber, L. A., 2004. Nonlinear Theory of Elasticity. Applications in Biomechanics. World Scientific Publishing Co.

[37] Wan, W., Dixon, J. B., Gleason, R. L., 2012. A strain energy function for arteries accounting for wall composition and structure. Biophys J 102, 2916–2925.

[38] Weizsäcker, H. W., Lambert, H., Pascale, K., 1983. Analysis of the passive mechanical properties of rat carotid arteries. J. Biomech. 16, 703–715.

[39] Zullinger, M., Fridez, P., Hayashi, K., Stergiopulos, N., 2004. A strain energy function for arteries accounting for wall composition and structure. J Biomech 37, 989–1000.

[40] Zullinger, M., Rachev, A., Stergiopulos, N., 2004. A constitutive formulation of arterial mechanics including vascular smooth muscle tone. Am J Physiol Heart Circ Physiol 287, H1335–H1343.

[41] Dayan, D., Hiss, Y., Hirshberg, A., Bubis, J. J. Wolman, M., 1989. Are the polarization colors of picrosirius red-stained collagen determined only by the diameter of the fibers?. Histochemistry 93(1), 27–29

[42] Farquharson, C., Robins, S. P., 1989. Immunolocalization of collagen types I and III in the arterial wall of the rat. The Histochemical Journal 21(3), 172–178

[43] Finlay, H. M., Canham, P. B., 1994. The layered fabric of cerebral artery fenestrations. Stroke 25(9), 1799-1806

[44] Finlay, H. M., Dixon, J. G., Canham, P. B.,1991. Fabric organization of the subendothelium of the human brain artery by polarized-light microscopy. Arteriosclerosis, Thrombosis, and Vascular Biology 11(3), 681–690 Histochemistry 93(1), 27–29

[45] Landuyt, M.,2006. Structural quantification of collagen fibers in abdominal aortic aneurysms. Master thesis, KTH Solid Mechanics, Stockholm, and Department of Civil Engineering, Gent.